Nano Research 2018, 11(11): 6086–6101
https://doi.org/10.1007/s12274-018-2126-5
Research Article
ISSN 1998-0124
CN 11-5974/O4

Drug targeting through platelet membrane-coated nanoparticles for the treatment of rheumatoid arthritis

Yuwei He[1,§], Ruixiang Li[1,§], Jianming Liang[1,2], Ying Zhu[1,2], Shuya Zhang[1], Zicong Zheng[1], Jing Qin[1], Zhiqing Pang[1] (✉), and Jianxin Wang[1] (✉)

[1] *Department of Pharmaceutics, School of Pharmacy, Fudan University & Key Laboratory of Smart Drug Delivery, Ministry of Education, Shanghai 201203, China*
[2] *Institute of Clinical Pharmacology, Guangzhou University of Traditional Chinese Medicine, Guangzhou 510006, China*
[§] *Yuwei He and Ruixiang Li contributed equally to this work.*

Received: 12 April 2018
Revised: 3 June 2018
Accepted: 8 June 2018

KEYWORDS
biomimetic nanoparticles, platelet membrane, rheumatoid arthritis, targeted drug delivery

ABSTRACT

The effective drug treatment of rheumatoid arthritis (RA) is hindered by poor delivery efficiency to the diseased site and the serious side effects caused by wide-spread drug distribution. Traditional drug-targeting strategies, such as ligand modification, are complex, laborious, and inefficient. Inspired by the intrinsic relationship between platelets and RA, platelet-mimetic nanoparticles (PNPs) were developed for targeted drug delivery in RA. Through platelet receptor-mediated adhesion, an intact platelet membrane was coated onto poly (lactic-co-glycolic acid) nanoparticles, endowing the resulting PNPs with various functional receptors. By coating with platelet membranes, the nanoparticles were stabilized and had a better circulation profile, providing a benefit for passive targeting. *In vitro* binding of PNPs to inflamed endothelium, and *in vivo* accumulation in joints of a collagen-induced arthritis (CIA) mouse model of RA were significantly improved via P-selectin and GVPI recognition, indicating that the PNPs could effectively target to RA tissues through multiple mechanisms, similar to natural platelets. Moreover, FK506, a model drug, was loaded into the PNPs and used to treat RA. Pharmacodynamic studies demonstrated that the FK506-PNPs had a notable anti-arthritic effect in CIA mice. This study provides a new biomimetic targeting strategy with great potential for the treatment of RA.

1 Introduction

Rheumatoid arthritis (RA) is one of the most common chronic autoimmune inflammatory disorders, leading to persistent inflammatory destruction of multiple joints, cartilage, and bone, even resulting in loss of joint function and severe disability [1]. The worldwide prevalence of RA has been estimated to be 1%, and there is a dramatic increase in its morbidity [2]. RA is a severe immune-mediated disease, and there is still

Address correspondence to Jianxin Wang, jxwang@fudan.edu.cn; Zhiqing Pang, zqpang@fudan.edu.cn

no cure for it. To reduce the signs and symptoms, patients have to follow long-term administration of anti-rheumatic drugs. These drugs are basically divided into four categories: disease-modifying anti-rheumatic drugs (DMARDs), glucocorticoids (GCs), nonsteroidal anti-inflammatory drugs (NSAIDs), and biologic drugs [3]. Despite remarkable progress in the clinical treatment of RA over the years, the therapeutic effect is still unsatisfactory because of poor drug accumulation at the inflamed site. In addition, the drugs commonly have severe, and even life-threatening side effects due to their non-specific distribution and long-term administration [3]. Therefore, novel drug delivery approaches are required to improve the targeting of therapeutic agents to effectively tackle these problems.

Some nanoscale drug delivery systems (DDS) have been explored for drug targeting in RA. Studies have shown that the submicron "gaps" between endothelial cells also exist in the RA synovium vasculature, leading to enhanced permeability of the diseased joint [4], similar to the well-known enhanced permeability and retention (EPR) effect in tumors. In this regard, nanoparticles could be widely used for drug delivery in RA, since they could effectively leak through the "gaps" and reach the inflamed joints. To further enhance the active targeting of nanoparticles, the most common approach is through ligand modification, using such ligands as folate [5], hyaluronic acid [6], and the RGD peptide [7]. These ligands can specifically bind to RA-associated cells, guiding nanoparticles to the RA site [8]. However, this chemical approach is complex, laborious, and inefficient. Since RA involves complex biological processes, the use of a single ligand limits the ability to guide nanoparticles. In addition, the currently used chemical modification process is complicated, which makes it infeasible for decorating nanoparticles with multiple ligands. Recently, the use of cell membrane-camouflaged nanoparticles, inspired by a biomimetic strategy, has emerged as a novel method to solve this bottleneck, and has aroused increasing attention [9]. These nanoparticles offer a simple and direct "Trojan horse" means to take advantage of the natural properties of various cells, including erythrocytes [10, 11], leukocytes [12], platelets [13–15], and even cancer cells [16], thereby promoting the therapeutic efficacy of the nanomedicine. By disguising the nanoparticle with a "uniform" made from a cell membrane, various functional proteins can be decorated onto the artificial nanoparticles, providing multiple pathways for the nanoparticles to take part in physiological and pathological processes. For example, erythrocyte membrane-camouflaged nanoparticles have been demonstrated to have an enhanced blood circulation time, which was ascribed to the presence of several RBC membrane proteins [17]. Nanoporous silicon particles coated with leukocyte membranes have been shown to be able to transport their payload across an inflamed endothelium and improve drug accumulation in tumors [12]. Compared with chemical modification, a cell-membrane cloaking technology can provide multiple functional molecules and ligands, using a much simpler process, and therefore could be a promising approach for drug targeting in RA.

Platelets are anucleated blood cells derived from megakaryocytes, which are abundant in the blood. The best-known function of platelets is to preserve the integrity of the vasculature and prevent bleeding [18, 19]. Besides their effect on hemostasis, unexpectedly, it has also been proven that platelets have important immunological and inflammatory functions [20]. In this regard, activated platelets can be found in the inflamed joint regions of RA patients, and act as an active player in the pathogenesis of RA. Mechanistically, platelets could amplify the inflammation in RA via the production of proinflammatory microparticles, which can elicit cytokine responses from fibroblast-like synoviocytes (FLS) via interleukin-1 production [21]. Highly abundant platelet microparticles (~ 100–1,000 nm) have been observed in synovial fluid samples from RA patients [21]. Besides passive leakage, the intermolecular interactions between activated platelets and inflammatory synovial tissues contribute significantly to the accumulation of platelet components in the inflamed joint in RA. CD44, a cell-surface glycoprotein, is up-regulated in inflamed synovial tissue cells (including macrophages, lymphocytes, lining cells, and fibroblasts) in RA, and the level of CD44 is related to the degree of synovial inflammation [22–24]. Activated platelets over-express P-selectin on their cell membranes, which binds

specifically to CD44 [25]; in addition, glycoprotein VI (GPVI), also on the platelet membrane, can interact with collagen IV [13], an abundant intercellular component in synovial tissues [4]. Consequently, platelet-mimetic nanoparticles might effectively facilitate RA targeting through multiple natural pathways.

Inspired by the intrinsic relationship between platelets and RA, we developed platelet membrane-coated poly(lactic-co-glycolic acid) (PLGA) nanoparticles (PNPs) for targeted drug delivery in RA (Scheme 1). By using platelet membranes, rather than platelets themselves, the targeting ability of the membrane proteins is retained intact, and the inflammatory component of the platelet can be eliminated. Here, the physicochemical characteristics of these PNPs were evaluated, and pharmacokinetic experiments were performed to assess the half-life of PNPs in circulation. The *ex vivo* tissue distribution of PNPs was also evaluated. The specific CD44 and collagen-targeting capability of these PNPs was confirmed both *in vitro* and *in vivo*, using a confocal imaging system and a near-infrared fluorescence (NIRF) imaging system. FK506, a potent immunosuppressive agent used for the treatment of RA patients failing methotrexate treatment, was used as a model drug and loaded into the PLGA nanoparticles by a nanoprecipitation process. For pharmacodynamic studies, the FK506-loaded PNPs were systemically administered to CIA mice to assess their anti-arthritic effect, using the arthritis index (AI), micro-CT imaging, and histological examinations as measures of efficacy. The safety of the PNPs was evaluated *in vivo* through hematology analysis and histological examination.

2 Experimental

2.1 Materials and animals

Prostaglandin E1 (PGE1) and FK506 were purchased from MedChemexpress (Monmouth Junction, NJ, USA). Protease inhibitors were purchased from Pierce Biotechnology Inc. (Rockford, IL, USA). Carboxyl

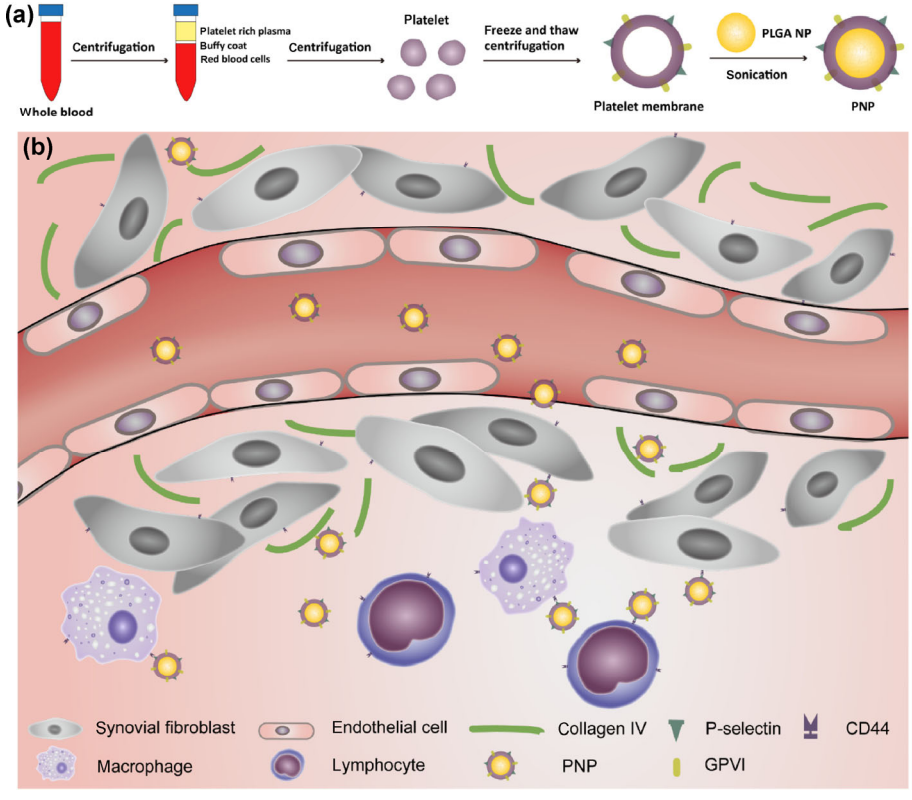

Scheme 1 Schematic illustration of the targeted delivery of PNPs to the inflamed joint in RA. (a) Process used for the preparation of platelet membrane-coated PLGA nanoparticles. (b) Targeted delivery of PNPs in the inflamed joint via enhanced permeability and specific binding of PNPs to collagen and overexpressed CD44 on some cells of the inflamed joint tissue.

group-terminated 50:50 poly(lactic-co-glycolic acid) (PLGA-COOH) was purchased from Lactel Absorbable Polymers (Pelham, AL, USA). FK506 enzyme linked immunosorbent assay (ELISA) kits were purchased from Abnova Co., Ltd. (Taiwan, China). 1,1′-dioctadecyl-3,3,3′,3′–tetramethylindodicarbocyanine, 4-chlorobenzenesulfonate salt (DiD) and 1,1′-dioctadecyl-3,3,3′,3′-tetramethylindotricarbocyanine iodide (DiR) were obtained from Fanbo Biochemical Co., Ltd. (Beijing, China). Collagen IV was purchased from Sigma-Aldrich (St. Louis, MO, USA). Bovine type II collagen (CII), complete Freund's adjuvant (CFA), and incomplete Freund's adjuvant (IFA) were all obtained from Chondrex, Inc. (Redmond, WA, USA). Carboxyfluorescein diacetate succinimidyl ester (CFDA-SE) and 4′,6-diamidino-2-phenylindole (DAPI) were purchased from Beyotime Biotechnology (Nantong, China). Pure water was produced from Milli-Q Integral (Merck, Germany). All other reagents were from Sinopharm Chemical Reagent Co. Ltd. (Shanghai, China).

Male SD rats (300–350 g), male ICR mice (20–22 g), and male DBA/1 mice (7 weeks old) were purchased from Sino-British SIPPR/BK Lab. Animal Co., Ltd. (Shanghai, China). All animal experiments were performed in accordance with the Guiding Principles for the Care and Use of Experimental Animals at Fudan University (Shanghai, China). The protocol of the animal experiments was approved by the Animal Experiment Ethics Committee of Fudan University.

2.2 Platelet isolation and membrane deviation

Platelets were isolated through differential centrifugation of whole blood, as previously described [13]. Briefly, whole blood was collected from SD rats via puncture of the abdominal aorta, using ethylenediaminetetraacetic acid (EDTA) as the anticoagulant. The blood was first centrifuged at 200 × *g* for 20 min at 22 ℃ (with no brake) to separate red and white blood cells. The supernatant was collected and spun at 100 × *g* for a further 20 min to pellet the contaminating red and white blood cells. To prevent platelet activation, 1 × PBS buffer containing 1 mM EDTA and 2 μM PGE1 was added to the resulting supernatant (platelet-rich plasma, PRP), and the platelets were then collected by centrifugation at 800 × *g* for 20 min at 22 ℃. Finally, the platelets were resuspended in 1 × PBS containing 1 mM EDTA and protease inhibitors. Platelet morphology was observed using a light microscope (ECLIPSE Ci, Nikon, Japan). The platelet suspension was counted using an automatic hematology analyzer (ADVIA 120 Hematology System, Siemens-Bayer, Germany) and then stored at −80 ℃.

Platelet membranes were extracted using a freeze-thaw process that was repeated seven times in total. Briefly, the platelet suspensions were frozen in liquid nitrogen, thawed in a water bath at room temperature, and then spun at 8,000 × *g* for 10 min at 4 ℃. After repeated washes with 1 × PBS solution containing protease inhibitors, the purified platelet membrane preparation was resuspended in water for further use.

2.3 Preparation of PNPs

FK506-loaded nanoparticle cores were first prepared by a nanoprecipitation process. Briefly, 5 mg of PLGA-COOH and 0.5 mg of FK506 were dissolved in 0.5 mL of acetone, and then the solution was injected into 1 mL of pure water. The mixture was placed in a vacuum at room temperature for 2 h to evaporate the acetone, and finally 5 mg·mL^{-1} of PLGA nanoparticle solution was obtained. The resulting NP solution was then filtered using an ultrafiltration centrifuge filter (molecular weight cutoff, 10 kDa). DiD or DiR dye-labeled PLGA nanoparticles (DiD-NPs or DiR-NPs) were prepared by the same nanoprecipitation process as described above, except that 0.5 mg of FK506 was replaced with 5 μg of DiD or DiR.

To prepare PNPs, the resulting PLGA nanoparticle solution was mixed with an equal volume of platelet membrane solution (1.5 × 10^{10} platelets·mL^{-1}) and sonicated for 3 min at room temperature using a bath sonicator (SG5200HE, Gutel, China) to fuse the platelet membrane onto the drug or dye-loaded nanoparticle cores [13].

2.4 Characterization of PNPs

The mean particle size, polydispersity index (PDI), and zeta-potential of platelet vesicles, NPs, and PNPs were determined using a dynamic light scattering (DLS) detector (Zetasizer, Nano-ZS, Malvern, UK). The morphology, size, and structure of the PNPs were

further examined by transmission electron microscopy (TEM, Tecnai G2 F20 S-Twin, FEI, USA). The samples were immobilized on carbon-coated copper grids and negatively stained with uranyl acetate (1%, w/v).

After platelet membrane coating, PNPs were centrifuged at 18,000 × *g* at 4 ℃ for 20 min. The amount of free FK506 in the supernatant was determined using an FK506 ELISA kit. After the supernatant was discarded, the PNPs in the deposit were lyophilized and weighed. The encapsulation efficiency (EE) and loading capacity (LC) were calculated using the following formulae

$$\text{EE}(\%) = \frac{\text{Drug imput} - \text{Free drug}}{\text{Drug imput}} \times 100\% \quad (1)$$

$$\text{LC}(\%) = \frac{\text{Drug imput} - \text{Free drug}}{\text{NPs}} \times 100\% \quad (2)$$

2.5 Platelet membrane protein analysis

The platelet membrane proteins present in PNPs were assessed by an SDS-PAGE electrophoresis assay. Briefly, PNPs were first spun down by centrifugation at 16,000 × *g* in 10% sucrose for 30 min. Following this, the membrane proteins present in the PNPs were extracted using a Membrane Protein Extraction Kit (Thermo Fisher Scientific, USA) and separated by electrophoresis on SDS-PAGE gels. Isolated platelets and purified platelet membranes were used as controls, and all samples were normalized for equal protein concentrations by the Bradford method. Two typical RA targeting-associated proteins, GPVI and P-selectin, were further examined by Western blotting. Primary antibodies, including sheep anti-mouse GPVI (R&D Systems, USA) and rabbit anti-mouse P-selectin (BioVision, USA) were used to stain GPVI and P-selectin, respectively. A donkey anti-rabbit IgG–horseradish peroxidase (HRP) conjugate (Jackson ImmunoResearch, USA) and a donkey anti-sheep IgG–HRP conjugate (Jackson ImmunoResearch) was used for secondary staining, respectively.

2.6 Analysis of stability of PNPs

The stability of PNPs in serum was measured by monitoring the ultraviolet absorbance at 560 nm, based on a previously published protocol [26]. Briefly, nanoparticles were suspended in fetal bovine serum (FBS) at a final nanoparticle concentration of 1 mg·mL^{-1}. The nanoparticles were then incubated at 37 ℃ and 150 rpm. Absorbance measurements were conducted in triplicate using a microplate reader (Infinite 200 PRO, Tecan, Switzerland) at different time points (0, 5, 15, 30, 45 min, and 1, 2, 4, 6, and 12 h) over a period of 12 h. Moreover, the stability of PNPs in PBS was also assessed. Briefly, PNPs were dispersed in 1 × PBS, and their average size was measured by DLS every day for 6 days. The EE of PNPs in PBS was also monitored every day for 6 days.

2.7 Analysis of *in vitro* drug release

Ten microliters of PNPs (1 mg·mL^{-1}) and 1 mL of release medium (1 × PBS containing 0.5% Tween 80 and 10% FBS) were added to a 1.5-mL EP tube, which was incubated at 37 ℃ and 100 rpm. Aliquots (n = 3) were withdrawn at regular intervals (0.5, 1, 2, 6, 12, 24, 36, 48, 72, and 96 h) and centrifuged at 18,000 × *g* for 20 min at 4 ℃. The FK506 concentration in the supernatant was analyzed using an FK506 ELISA kit per the manufacturer's instructions. The accumulated drug release from the PNPs was plotted against time.

2.8 Cell culture

The human rheumatoid arthritis synovial cell line (MH7A) was a kind gift from Dr. Xiaoyan Shen, Fudan University (Shanghai, China). The cells were cultured in Dulbecco's Minimum Essential Medium (Corning, NY, USA) supplemented with 10% fetal bovine serum (Gibco, NY, USA), 1% penicillin (100 IU·mL^{-1}, Corning), and streptomycin (100 μg·mL^{-1}, Corning).

2.9 *In vitro* binding test

As previously described [13], collagen IV (Sigma-Aldrich, USA) was reconstituted in 0.25% acetic acid to a concentration of 2 mg·mL^{-1}. Following this, 500 μL of the collagen solution was added to a glass-bottomed cell culture dish and incubated in a fume hood overnight to remove the solvent. The collagen-coated cell culture dish was then used to seed the MH7A cells, which were cultured for 24 h. The dish was then incubated with 1 mg·mL^{-1} DiD-labeled PNPs

(DiD-PNPs) at 4 °C for 5 min, and then washed three times with 1 × PBS. The cell nuclei were stained with 5 μg·mL^{-1} DAPI for 15 min, and then washed three times with 1 × PBS. The cell cytosol was stained with 5 μg·mL^{-1} CFDA-SE for 15 min, after which cell staining was stopped by the addition of cell culture medium. The sample was fixed in 4% paraformaldehyde for 30 min at room temperature, and observed by confocal microscopy (Carl Zeiss LSM710, Germany).

2.10 Establishment of the RA induction model

The CIA animal model was established in DBA/1 mice per the manufacturer's instructions (Chondrex, USA). Briefly, bovine type II collagen was dissolved in 0.1 M acetic acid at 4 °C (2 mg·mL^{-1}) and then emulsified with an equal volume of CFA containing 2 mg·mL^{-1} *Mycobacterium tuberculosis*. Mice were then immunized subcutaneously at the base of the tail with 100 μL of the emulsion. On day 21 after primary injection, the mice received a booster injection with collagen II emulsified in IFA.

2.11 Pharmacokinetic analysis of PNPs

Pharmacokinetics experiments were performed on male ICR mice (20–22 g). To monitor the circulation half-life of PNPs, 200 μL of DiD-PNPs were injected into the tail vein of the mice. Fifty microliters of blood was collected by cheek pouch puncture at 1, 5, 15, 30 min, and 1, 3, 8, and 24 h following injection. As a comparison, DiD-NPs containing the same dose of DiD was also tested in parallel. Each experimental group had five mice. The collected blood samples were diluted with 50 μL of 1 × PBS in a 96-well plate before fluorescence measurement (640/670 nm).

2.12 *In vivo* imaging and *ex vivo* tissue distribution of PNPs

The *in vivo* accumulation of PNPs at the arthritis joints was visualized by NIRF imaging. Briefly, DiR-labeled PNPs (DiR-PNPs) were injected into the tail vein of normal DBA/1 or CIA mice in order to observe the biodistribution of PNPs *in vivo*. The NIRF images were obtained at five different time points (1, 2, 6, 12, and 24 h) after injection, using an *in vivo* imaging system (IVIS Spectrum, Caliper, USA). To examine the *ex vivo* tissue distribution of PNPs, the major organs and joints were dissected from CIA mice 24 h after DiR-PNPs injection and imaged using an *in vivo* imaging system. The tissue distribution of the PNPs was quantified by measuring the average of the NIRF intensity in the regions of interest (ROI), using the living image software.

2.13 Analysis of localization of PNPs in inflammatory synovial tissue

To examine the localization of PNPs in inflammatory synovial tissue, DiD-PNPs were injected intravenously into the tail vein of CIA mice. Normal mice were used in parallel as a control. Two hours later, the mice were sacrificed, and the synovial tissue was removed, fixed in 4% paraformaldehyde for 24 h, and dehydrated in a 30% sucrose solution until subsidence. Frozen sections of 10-μm thickness were prepared and blocked with 10% BSA at room temperature for subsequent immunostaining. CD44 and collagen were labeled with a rabbit polyclonal anti-CD44 antibody (1:1,000; Abcam, USA) and a rabbit polyclonal anti-collagen IV antibody (1:1,000; Abcam), respectively. Afterwards, the slices were treated with an Alexa Fluor 555-labeled donkey anti-rabbit IgG (1:1,000; Invitrogen, USA). DAPI was used to stain nuclei. The fluorescence images were visualized with a confocal microscope (Carl Zeiss LSM710, Germany).

2.14 Analysis of *in vivo* therapeutic efficacy

One week after the second immunization, mice with disease onset (AI > 3) were randomly assigned to four groups (five mice per group) and were intravenously administered with saline, free FK506 (an aqueous solution containing 6% cremophor EL and 6% ethanol), FK506-NPs, or FK506-PNPs at an FK056 dose of 1 mg/kg body weight once every other day for 2 weeks. Healthy DBA/1 mice without any treatment were used as a negative control group.

Paw inflammation was scored visually every other day based on the published standard as follows [27]: 0 = normal paw; 1 = one toe inflamed and swollen; 2 = more than one toe, but not entire paw inflamed and swollen, or mild swelling of entire paw; 3 = erythema

and moderate swelling extending to entire paw; and 4 = most severe erythema and swelling for the whole paw and ankle. Each paw was graded with a score from 0 to 4, creating an arthritis score on a scale of 0–16 for each individual mouse.

2.15 Micro-computed tomography (Micro-CT) analysis

After treatment, the therapeutic efficacy of the PNPs was analyzed by micro-CT, as previously described [7, 28, 29]. Briefly, the isolated hind paws from each mouse were fixed in 4% paraformaldehyde for 24 h, and then scanned using a micro-CT imaging system (Skyscan 1176, Beckman Coulter, USA). The micro-CT scanning parameters were as follows: Voltage, 50 kV; current, 497 μA; resolution, 18 μm; and aluminum filter, 0.5 mm. Scanned images were reconstructed into three-dimensional structures using CT-Vol software (Skyscan), and these images were further analyzed using CTvox Version 2.7 software (Skyscan) to produce a visual representation of the data.

2.16 Histological analysis

The mice were sacrificed at the end of the treatment, after which hind paws were removed for histology. Specifically, the paws were fixed in 4% paraformaldehyde for 48 h, and then decalcified with PBS containing 15% EDTA at room temperature. Once decalcification was complete, the samples were washed with water, dehydrated again with a graded ethanol series, and embedded in paraffin. Tissues were sliced into 4-μm-thick sections and stained with hematoxylin and eosin (H&E). Images of the sections were obtained by optical microscopy. For immunohistochemical analysis, sections were incubated with specific antibodies directed against TNF-α, IL-1β, or IL-6 followed by incubation with the appropriate secondary antibodies.

2.17 Analysis of *in vivo* safety of PNPs

To assess the biocompatibility of PNPs, ICR mice (n = 6) were injected with 200 μL of PNPs (2.5 mg·mL^{-1}) every other day for a week. Following this, whole blood was collected using an anticoagulation tube 24 h after the last treatment and examined using an automatic hematology analyzer. Mice receiving an equivalent volume of PBS were treated in parallel for comparison.

To evaluate the potential toxicity of FK506-PNPs, CIA mice were sacrificed after treatment, and the liver, spleen, and kidney were harvested. The tissues were fixed in 4% paraformaldehyde for paraffin sectioning followed by H&E staining to evaluate the histopathological changes due to toxicity.

2.18 Statistical analysis

Values are presented as the mean ± SD, or the mean ± SEM, as indicated, and the data were analyzed using GraphPad Prism 6.0 (GraphPad Software, CA, USA). Differences were assessed by a one-way analysis of variance followed by Newman–Keuls post-hoc test for multiple groups and a Student's t test between two groups. A value of $P < 0.05$ was considered to indicate statistical significance.

3 Results and discussion

3.1 Platelet isolation and membrane purification

Before platelet isolation, whole blood was anti-coagulated with EDTA to prevent platelet aggregation. The platelets were isolated from rat whole blood by differential centrifugation, and strong mechanical forces were avoided to prevent platelet activation. Furthermore, PEG1 was added as a platelet activation inhibitor. Under a light microscope, the isolated platelets were visible as small round highlights. The final platelet suspension was counted using an automatic hematology analyzer, resulting in a yield of 5×10^8 platelets·mL^{-1} rat blood. The hematology analysis revealed that there was almost no contamination with other blood cells (Table S1 in the Electronic Supplementary Material (ESM)). The platelet membrane was purified by punching the platelets through repeated freeze-thaw and centrifugation.

In the event that a scale-up isolation of platelet membranes is required, there is a reliable source of platelets; platelet transfusions have been in medical use since the 1950s [30], and are extensively used to treat or prevent bleeding in the clinic. In addition, increasing number of studies have shown the

biointerface between platelets and various diseases [15]. Platelets have many unique biological functions, having a great potential as an ideal biomaterial for drug delivery in translational medicine.

3.2 Characterization of PNPs

Platelet membranes can be fused onto the surface of PLGA NPs (Scheme 1(a)) by water-bath sonication for a short time, as has previously been reported [13]. The average hydrodynamic diameter of the resultant PNPs was determined to be 122.3 nm by DLS (Fig. 1(a)). The NPs had a narrow size distribution, while the PDI value of PNPs were slightly larger, probably due to the presence of the platelet membranes (Fig. 1(b)). After platelet membrane coating, the zeta potential value of the NPs (−42.5 mV) increased to −24.7 mV, which was similar to that of the surface charge of platelet membrane vesicles (−25.6 mV) (Fig. 1(c)), suggesting a successful coating of platelet membranes on the NPs. These results revealed that the final PNPs were about 20 nm larger than the bare NPs (103.0 nm) (Fig. 1(d)), and that the increased size was in accordance with the thickness of the platelet cell membrane. The presence of the platelet membrane on the nanoparticle surface was further verified by morphological examination by TEM (Fig. 1(e)), which showed a complete and unilamellar coating surrounding the spherical NP cores. FK506 was encapsulated into the PNPs with a remarkably high EE of 96.7 ± 1.8% and an LC yield of 8.8 ± 0.16%, which can probably be attributed to the relatively high lipophilicity of FK506 (log*P* 3.3). The high oil/water partition coefficient of FK506 drug suggests a strong interface with the carrier material (PLGA), resulting in a high load. Based on this, we suggest that other drugs with a high log*P* value could also be easily

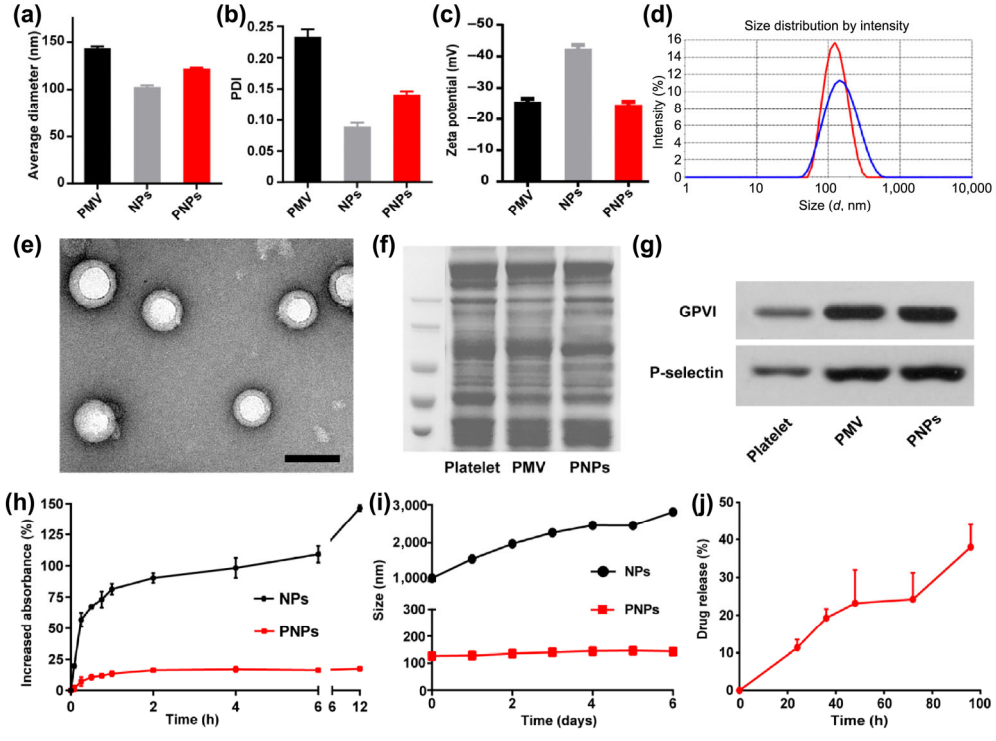

Figure 1 Preparation and characterization of PNPs. (a) The mean hydrodynamic diameters of platelet membrane vesicle (PMV), NPs, and PNPs based on dynamic light scattering (n = 3; mean ± SD). (b) The PDI of PMV, NPs, and PNPs (n = 3; mean ± SD). (c) Surface zeta potential of PMV, NPs, and PNPs (n = 3; mean ± SD). (d) Size distribution of NPs and PNPs based on dynamic light scattering (blue: PNPs; red: NPs). (e) TEM image of PNPs negatively stained with uranyl acetate. Scale bar, 100 nm. (f) Protein profiles of the platelet, PMV, and PNPs assessed using SDS-PAGE electrophoresis. (g) Western blotting analysis of targeting- related proteins (GPVI and P-selectin) on the platelet membrane. (h) Stability of PNPs and bare NPs in fetal bovine serum monitored by absorbance at 560 nm (n = 3; mean ± SD). (i) Stability of PNPs and bare NPs in PBS monitored by DLS (n = 3; mean ± SD). (j) Drug release profiles of FK506-loaded PNPs (n = 3; mean ± SD).

encapsulated within this delivery system.

SDS-PAGE electrophoresis revealed that the protein composition of the platelet membrane was mostly retained in the PNPs (Fig. 1(f)), indicating there was no evident loss of platelet membrane proteins during PNP preparation. In addition, two proteins typically associated with targeting strategies (GPVI and P-selectin) were observed to be present by Western blotting (Fig. 1(g)). The retention of these proteins provides the nanovesicles with a basis for directing their biological function. Through this simple and direct coating method, these synthetic particles were able to permanently inherit a complex membrane protein system, which would be impossible by chemical methods.

3.3 *In vitro* stability and drug release of PNPs

To test the stability of PNPs in serum, the absorbance at 560 nm of NP or PNP solutions was monitored at 37 °C in serum as a function of time (Fig. 1(h)). The absorbance of PNPs increased slightly over 12 h, indicating that there was no obvious particle aggregation. In comparison, the absorbance of the bare NPs increased sharply in only 15 min. The stability of PNPs in PBS was also assessed over a longer duration. As shown in Fig. 1(i), PNPs showed a slight increase in size over 6 days, whereas the NPs immediately aggregated in PBS. The EE of PNPs in 1 × PBS over 6 days indicated that little FK506 leaked out from the PNPs during the experiment (Fig. S1 in the ESM). Therefore, these results suggest that coating the platelet membrane onto PLGA nanoparticles was able to improve the stability of the NPs both in FBS and in PBS. The *in vitro* release profile of FK506 from PNPs in 1 × PBS containing 10% serum and 0.5% Tween 80 showed that only 40% of FK506 was released from the PNPs in 96 h (Fig. 1(j)). This sustained release profile might be due to the strong interaction between PLGA and FK506, suggesting that it might be beneficial as an RA-targeting therapy.

3.4 *In vitro* binding capacity of PNPs

Fibroblast-like synoviocytes (FLSs) and the extracellular matrix (ECM) elaborated by these cells are important components of the synovial membrane tissue. Here, collagen IV-coated dishes seeded with MH7A cells were used to simulate synoviocytes and their ECM. The interaction of PNPs with this synovial membrane was then explored using this *in vitro* model. A large amount of PNPs could adhere to the intercellular collagen IV (Fig. 2), probably owing to the specific affinity between collagen and GPVI on the platelet membrane, as previously reported [13]. These *in vitro* binding results suggest that PNPs could potentially be targeted to collagen IV *in vivo*.

3.5 RA-targeting ability, pharmacokinetics, and biodistribution of PNPs

To evaluate the specific targeting of PNPs to inflamed tissues in RA, DiR solution, DiR-labeled NPs, or PNPs were injected intravenously into CIA mice (n = 3). Each model mouse had both non-inflamed (left) and inflamed (right) hind paws. The fluorescence signals in the hind paws were monitored as a function of time, using the NIRF imaging system (Fig. 3(a)). Real-time imaging revealed that the NIRF intensity of the hind

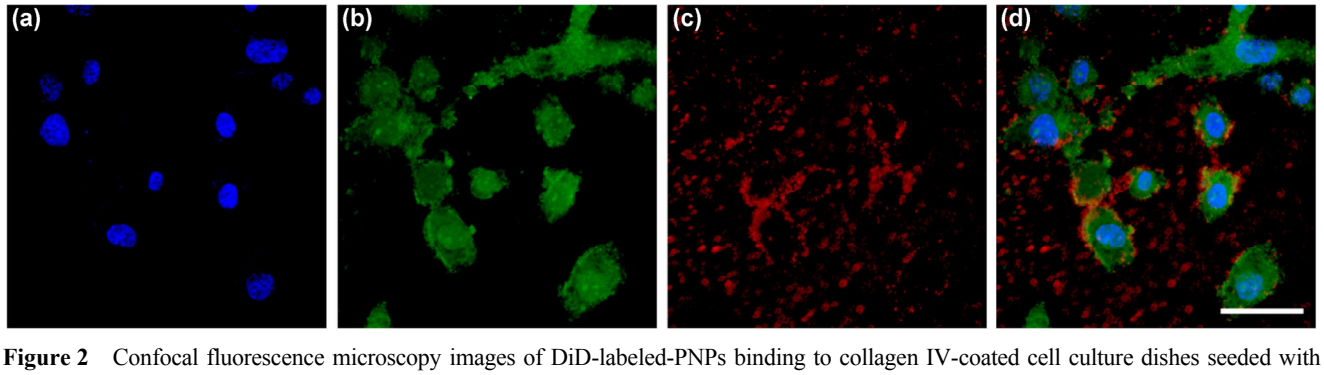

Figure 2 Confocal fluorescence microscopy images of DiD-labeled-PNPs binding to collagen IV-coated cell culture dishes seeded with MH7A cells (a) MH7A cells (nuclei stained in blue). (b) MH7A cells (cytosol stained in green). (c) DiD-labeled-PNPs (red). (d) Merge. Scale bar, 50 μm.

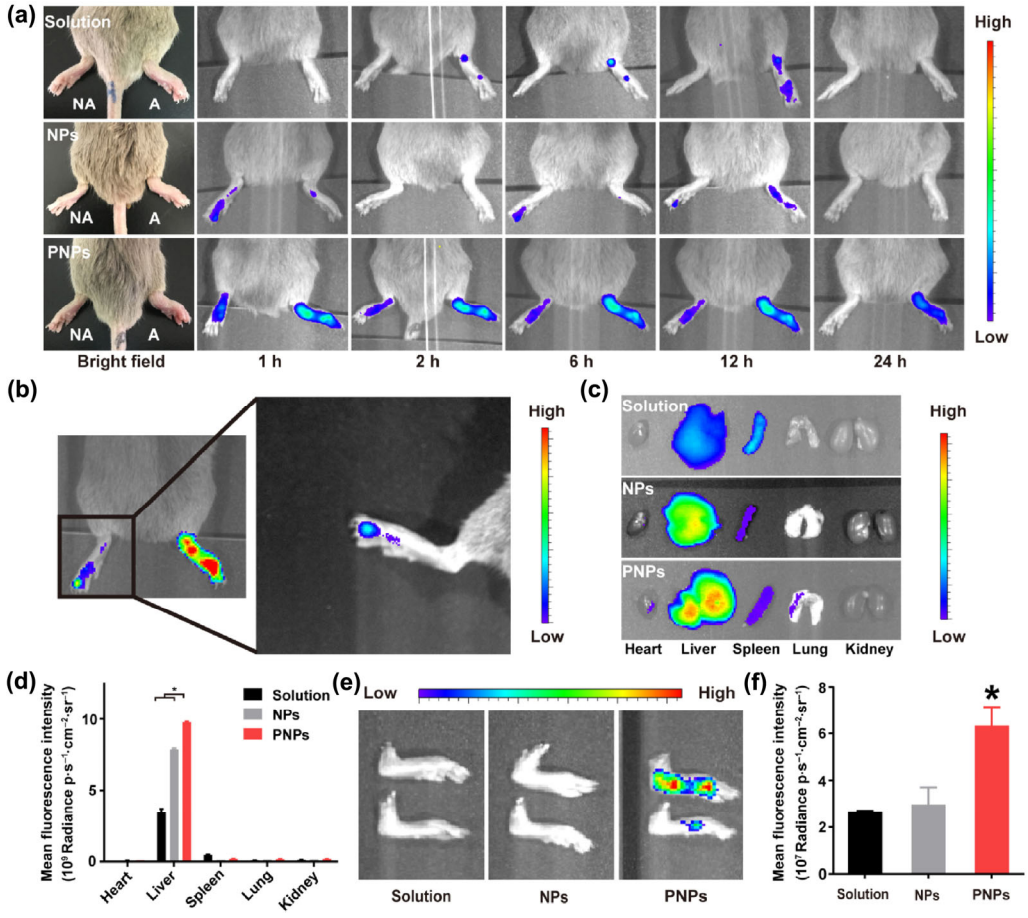

Figure 3 *In vivo* and *ex vivo* imaging of PNPs in CIA mice. (a) *In vivo* NIRF of both non-arthritic paws (left, NA) and arthritic paws (right, A) in CIA mice (n = 3) at different time points after intravenous injection. (b) Fluorescence images taken of an inflamed right paw with just one arthritic toe. The CIA mouse was treated with DiD-labeled-PNPs. (c) *Ex vivo* NIRF imaging of major organs 24 h post nanoparticle injection. (d) Mean NIRF intensity of major organs (n = 3; mean ± SD), $P < 0.05$ versus solution or the NP group. (e) *Ex vivo* NIRF image of inflamed paws from the NP and PNP groups 24 h post injection. (f) Mean NIRF intensity of inflamed paws (n = 3; mean ± SD), $P < 0.05$ versus solution or the NP group.

paws in the PNP group was much higher than that for either the DiR solution group or the NP group. In the PNP group, the NIRF signal gradually increased, and reached a peak at 12 h in the inflamed hind paws. For each mouse in the PNP group, the fluorescence signal in the inflamed paw was significantly higher than that in the non-inflamed paw, indicating that PNPs selectively accumulated in the inflamed joint. In contrast with normal toes, the inflamed toes (Fig. 3(b)) showed much higher fluorescence, demonstrating the accurate and high amount of accumulation of PNPs in inflamed tissue. Intraarticular injection is one direct and accurate way for targeted delivery of a drug in RA. However, since RA leads to the persistent inflammatory destruction of multiple joints, multi-site targeting is needed. This smart DDS using PNPs is therefore likely to have much better patient compliance compared with intraarticular injection.

The DiD dye was used to label nanoparticles to study the pharmacokinetics of PNPs, as previously described [13]. Figure S2 in the ESM shows that the PNPs had much longer blood retention times than bare NPs, indicating that the platelet membrane coating was able to stabilize the NP cores *in vivo*, and improve the circulation time, which is consistent with the results of the *in vitro* stability test. The biodistribution of the NPs and PNPs in major organs and inflamed paws was further investigated in CIA mice 24 h post injection. Similar to other nanoparticle systems, both the NPs and PNPs were found to be mainly distributed to

the liver and spleen (Figs. 3(c) and 3(d)), most likely as result of the uptake by phagocytic cells in the reticuloendothelial system (RES). Moreover, the distribution of PNPs in the liver and spleen was also in accordance with the physiological clearance pathways for platelets, as has previously been reported [31]. The fluorescence signal in the excised inflamed paws in the PNP group were much stronger than that in the NP group (Fig. 3(e)). Quantitation indicated that the amount of PNPs in the inflamed joints in the CIA mice was 2.1 times higher than that in the NP group (Fig. 3(f)). These results demonstrate that platelet membrane coating allows the nanoparticles to preferentially accumulate at the sites of joint inflammation. This improvement in targeting efficiency probably arises owing to two aspects: the first is the stabilization effect of the membrane coating, and the second is related to the intermolecular interactions between the activated platelets and the inflamed synovial tissues.

3.6 Localization of PNPs in inflamed synovial tissue

Immunofluorescence was used to examine the localization of PNPs in the inflamed synovial tissue, as well as to explore the potential targeting mechanism of the PNPs. CD44 was found to be overexpressed in the synovial tissue in CIA mice, and there was a substantial accumulation of PNPs in the inflamed synovial tissue, with the PNPs primarily co-localizing with CD44 (Fig. 4(a)). In contrast, few PNPs were founded in the synovial tissue from normal mice. The synovial lining is composed of fibroblast-like type B and macrophage-like type A lining cells, with the intercellular space containing structural components, including collagen [32]. Figure 4(b) shows the collagen

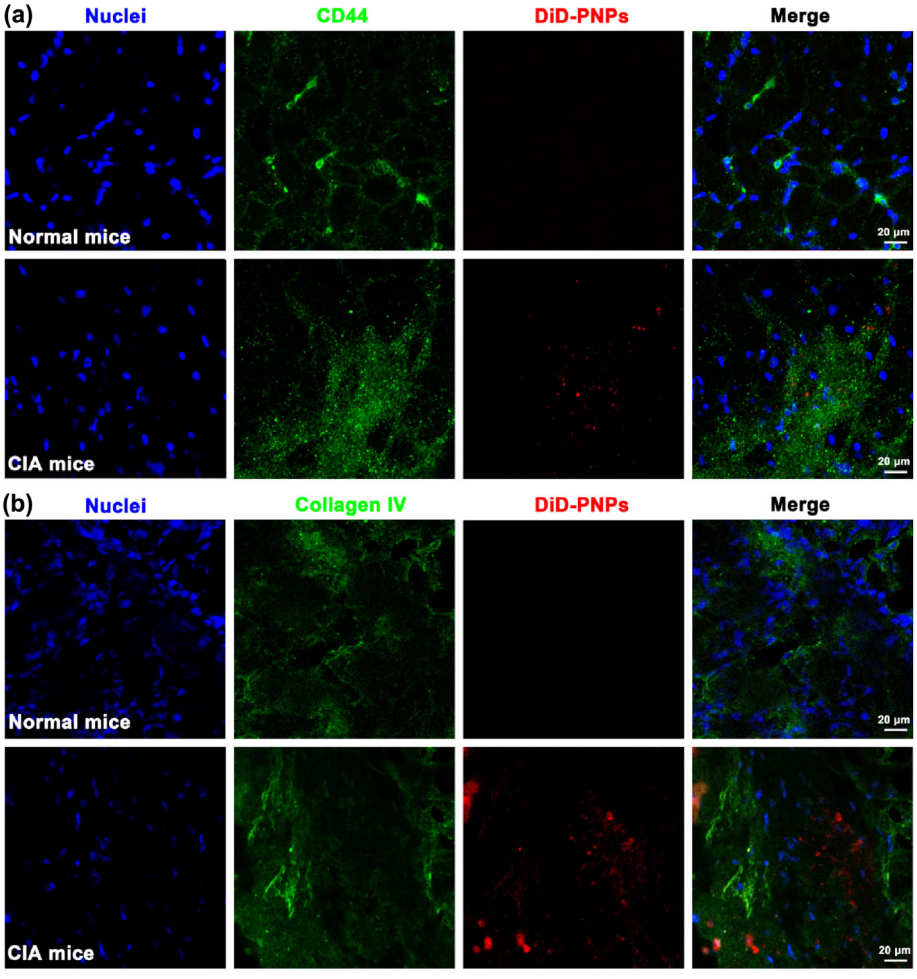

Figure 4 Confocal fluorescence images of DiD-labeled-PNPs (red) in synovial tissue. Nuclei were counterstained with DAPI (blue). Immunofluorescence staining was performed for (a) CD44 (green) or (b) collagen (green), separately. Scale bar, 20 μm.

present in the intercellular space. A significant number of PNPs were found to be co-localized with collagen in CIA mice, whereas very few PNPs were found to co-localize with collagen in normal mice. Upon platelet membrane coating, the nanoparticles acquire multiple complex membrane components. It is likely that the targeting effect is an integrated result of several comprehensive mechanisms, so, in addition to the pathway explored here, it is likely that other mechanism for co-localization exists, and this will require further investigation.

3.7 *In vivo* therapeutic efficacy of PNPs

Collagen-induced arthritis in DBA/1 mice is the most widely used autoimmune model of RA, since it demonstrates similar immunological and pathological features with human RA [33]. In the present study, therapeutic treatment was initiated at the onset of arthritis (arthritis index (AI) of each mouse > 3), with the initial mean AI not being significantly different between groups. Seven days after the second immunization, the CIA mice were treated with FK506-PNPs every other day for 2 weeks. The changes in the AI are shown in Fig. 5(a). Compared with PBS-treated mice, all other groups showed a significantly decreased AI. However, there was no significant difference in AI between free FK506 and FK506-NPs. This is not a surprising result, because previous studies have shown that NPs are not stable in serum [34], and therefore cannot effectively accumulate in inflamed joints. Notably, the PNP group had the lowest AI among all the groups over the whole treatment time, which could be attributed to the high accumulation of PNPs in the inflamed joints. In addition, mice in the FK506-PNP group had significantly lower degrees of redness or swelling in the hind limbs compared with

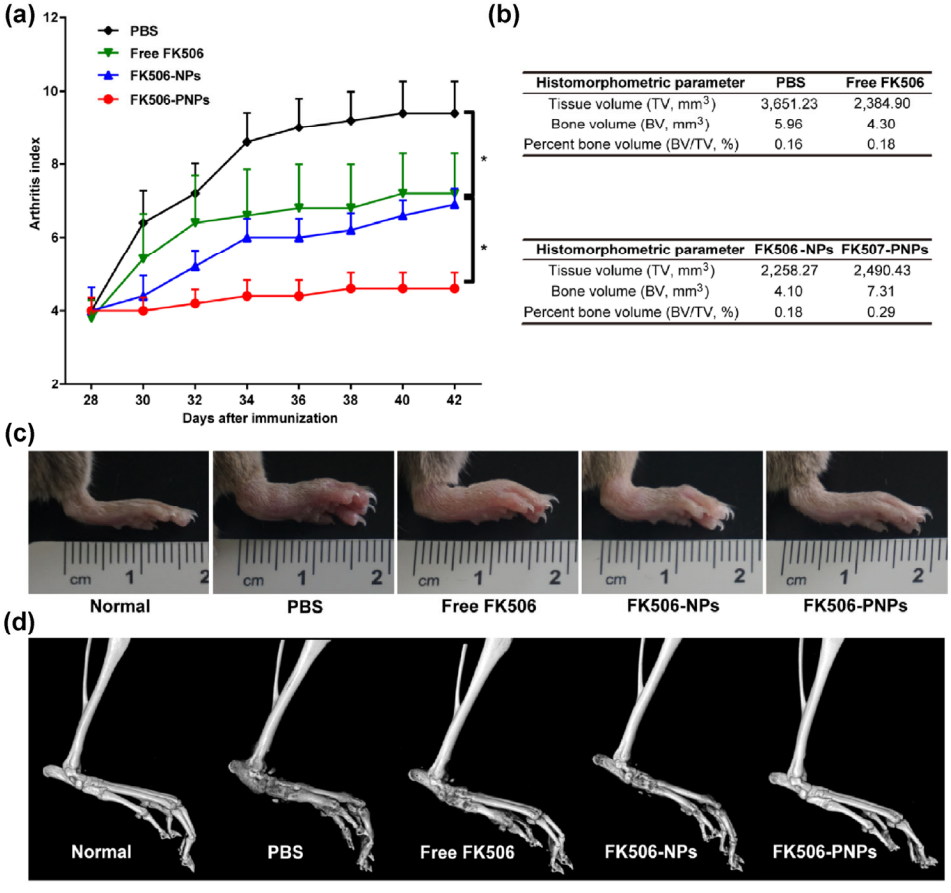

Figure 5 Therapeutic efficacy in CIA mice. (a) Mean arthritis index of rheumatoid arthritis as a function of time after first immunization. Values are mean ± SEM (n = 5). $P < 0.05$ versus PBS, free FK506 or FK506-NPs. (b) Quantitative analysis of the hind paw micro-CT data. (c) Representative photographs of hind paws from CIA mice in different treatment groups and normal mice without any treatment. (d) Three-dimensional reconstruction of micro-CT images of the hind paws of normal mice and CIA mice in different treatment groups.

other groups (Fig. 5(c)). Similar results could also be seen in the representative photographs taken of the fore paws (Fig. S3 in the ESM). FK506 is an immunosuppressive drug, which is used for the treatment of RA patients who respond insufficiently to other drugs [35].

3.8 Microcomputed tomography analysis

Bone erosion is a central pathological feature in RA, and is often used to monitor the severity of the disease [36]. Micro-CT was used to further test bone changes in each of the treatment groups. As shown in Fig. 5(d), there was obvious severe bone destruction, including rough bone surfaces and severe bone erosion, in the joints of mice in the PBS, free FK506, or FK506-NP groups. Prominent bone erosions were evident on the calcaneus bone and extended to the metatarsals in these three groups. In contrast, only minor erosions were seen in these areas within the ankle joints of the FK506-PNP-treated mice, demonstrating that FK506-PNPs produce an impressive reduction in the extent of ankle joint bone erosion, resulting in bones that were similar to those in normal mice. A quantitative analysis of the hind paw micro-CT data was shown in Fig. 5(b).

3.9 Histological analysis

The therapeutic effect of PNPs was further evaluated by examining inflammation and tissue destruction in both bone and cartilage using H&E staining and immunohistochemical staining to examine tissue histology. Ankle joint sections were prepared at the end of the therapy to examine bone and cartilage preservation, and the level of several inflammatory cytokines. As shown in the uppermost panel of Fig. 6, joint sections from CIA mice treated with PBS showed severe bone and cartilage erosion with pannus formation, while normal mice without CIA induction showed no destruction of bone or cartilage. The joint sections from the free FK506 and FK506-NP groups showed intermediate inflammation. Compared with these groups, there was no obvious bone or cartilage erosion, nor any pannus tissue formation in the FK506-PNP group. An immunohistochemical analysis showed that, compared with normal mice, the expression levels of TNF-α, IL-6, and IL-1β were significantly increased around the joints in the PBS, free FK506, and FK506-NP groups. In contrast, the expression of these cytokines was significantly decreased in the FK506-PNP group (Fig. 6 and Fig. S4 in the ESM), with levels being similar to those found

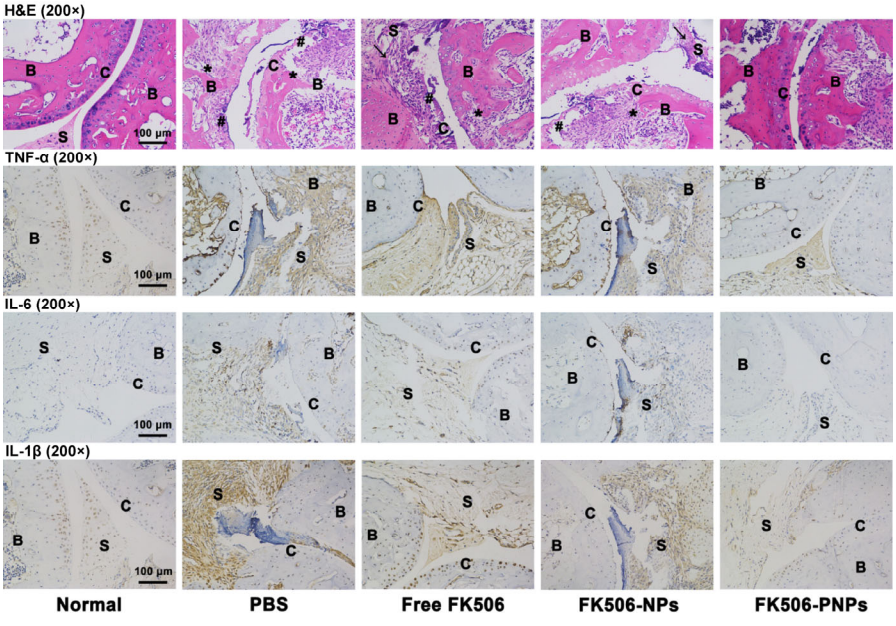

Figure 6 Histological analysis of dissected ankle joint tissues of normal mice and CIA mice in different treatment groups. Representative images of ankle joints (B: bone, C: cartilage, S: synovial tissue) revealed varying degrees of inflammation and pannus formation (arrows) with cartilage destruction and bone destruction (*) in PBS, free FK506 and FK506-NP, and FK506-PNP-treated CIA mice (H&E staining, 200 ×). Images of immunohistochemical staining (200 ×) for TNF-α, IL-6, and IL-1β.

in normal mice. From these data, we hypothesize that there is a high degree of accumulation of FK506-PNPs in the inflamed joints in this RA model resulting in a large reduction in paw swelling, bone erosion, and inflammation.

3.10 Safety of PNPs

In the clinic, platelets are one of the most frequently used blood products. Studies have shown that pure platelets do not provoke a primary immune response, and since platelets have only blood related antigens they only have low immunogenicity, similar to that seen for RBCs [37]. To evaluate the biocompatibility of PNPs, a hematological analysis was performed (Fig. 7(a)). There was no significant difference between the PNP group and the control group, suggesting that PNPs have excellent biocompatibility. Since the bio-distribution study showed a relatively high accumulation of PNPs in the liver and spleen, a histological examination of the liver and spleen was performed after treatment to examine any potential

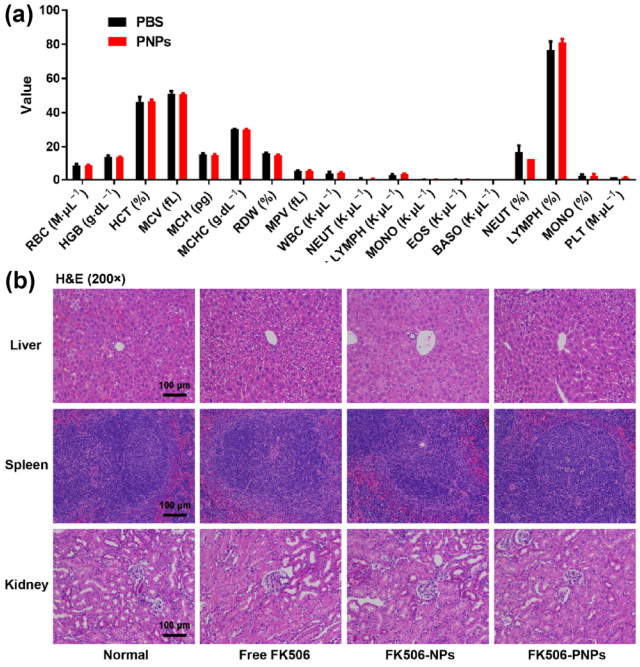

Figure 7 Preliminary safety evaluation. (a) Evaluation of the safety of PNPs in healthy mice. Healthy ICR mice were intravenously injected with PBS or PNPs every other day for a week. Blood hematology tests were performed. (b) Histological examination of typical organs, including liver, spleen, and kidney, from CIA mice after treatment with PBS or PNPs compared with normal mice.

in vivo toxicity of the FK506-PNPs. In addition, kidney tissue was also examined owing to the reported potential kidney toxicity of FK506. H&E staining indicated that the FK506-PNPs produced negligible changes in tissue architecture compared with that in normal mice without any treatment, implying there is little toxicity of the FK506-PNPs after treatment at multiple doses (Fig. 7(b)).

4 Conclusions

We developed platelet membrane-coated PLGA nanoparticles for targeted drug treatment of RA. Upon disguising the nanoparticles with a "uniform" using a natural cell membrane, the synthetic NPs were able to acquire biological functions similar to platelets. The studies demonstrated the accurate and significant accumulation of PNPs in the inflammatory synovial tissue, which could be partly attributed to the interaction of platelet membrane proteins (GPVI, P-selectin) on the PNPs with collagen IV, and the overexpression of CD44 in RA synovial tissue. A pharmacodynamic study showed that FK506-PNPs can significantly control RA progression in the CIA mouse model of RA, and a preliminary safety study demonstrated the excellent biocompatibility of PNPs. Increasing numbers of platelet-related drug delivery platforms have been developed in recent years [38–40], and so platelets show great prospects as functional natural materials. By integrating the natural cell membrane with the biodegradable artificial material PLGA, this biomimetic strategy has great potential in clinical applications [13, 14]. Since chronic inflammation is now recognized to be a cause, or agitator, of various diseases, and platelets play an important role in pathological processes of inflammation, this platform may also hold great promise for the treatment of other inflammation-related diseases.

Acknowledgements

We acknowledge the financial support of the National Natural Science Foundation of China (Nos. 81690263, 81472757, 81361140344, 81773283, and 81773911). Thanks are given to Dr. Yang Yang from Shanghai University

of Traditional Chinese Medicine for his kind help with the CIA model.

Electronic Supplementary Material: Supplementary material (including platelet purity test, changes of EE of PNPs, pharmacokinetic study, photographs of fore paws from normal mice and inflamed mice, and quantitative analysis of the inflammatory cytokines) is available in the online version of this article at https://doi.org/10.1007/s12274-018-2126-5.

References

[1] Mitragotri, S.; Yoo, J. W. Designing micro- and nano-particles for treating rheumatoid arthritis. *Arch. Pharm. Res.* **2011**, *34*, 1887–1897.

[2] Scott, D. L.; Wolfe, F.; Huizinga, T. W. J. Rheumatoid arthritis. *Lancet* **2010**, *376*, 1094–1108.

[3] Yuan, F.; Quan, L. D.; Cui, L.; Goldring, S. R.; Wang, D. Development of macromolecular prodrug for rheumatoid arthritis. *Adv. Drug Deliv. Rev.* **2012**, *64*, 1205–1219.

[4] Cloutier, N.; Paré, A.; Farndale, R. W.; Schumacher, H. R.; Nigrovic, P. A.; Lacroix, S.; Boilard, E. Platelets can enhance vascular permeability. *Blood* **2012**, *120*, 1334–1343.

[5] Chandrasekar, D.; Sistla, R.; Ahmad, F. J.; Khar, R. K.; Diwan, P. V. The development of folate-PAMAM dendrimer conjugates for targeted delivery of anti-arthritic drugs and their pharmacokinetics and biodistribution in arthritic rats. *Biomaterials* **2007**, *28*, 504–512.

[6] Heo, R.; Park, J. S.; Jang, H. J.; Kim, S. H.; Shin, J. M.; Suh, Y. D.; Jeong, J. H.; Jo, D. G.; Park, J. H. Hyaluronan nanoparticles bearing γ-secretase inhibitor: *In vivo* therapeutic effects on rheumatoid arthritis. *J. Control. Release* **2014**, *192*, 295–300.

[7] Lee, S. M.; Kim, H. J.; Ha, Y. J.; Park, Y. N.; Lee, S. K.; Park, Y. B.; Yoo, K. H. Targeted chemo-photothermal treatments of rheumatoid arthritis using gold half-shell multifunctional nanoparticles. *ACS Nano* **2013**, *7*, 50–57.

[8] Yang, M. D.; Feng, X. R.; Ding, J. X.; Chang, F.; Chen, X. S. Nanotherapeutics relieve rheumatoid arthritis. *J. Control. Release* **2017**, *252*, 108–124.

[9] Luk, B. T.; Zhang, L. F. Cell membrane-camouflaged nanoparticles for drug delivery. *J. Control. Release* **2015**, *220*, 600–607.

[10] Hu, C. M. J.; Fang, R. H.; Copp, J.; Luk, B. T.; Zhang, L. F. A biomimetic nanosponge that absorbs pore-forming toxins. *Nat. Nanotechnol.* **2013**, *8*, 336–340.

[11] Su, J. H.; Sun, H. P.; Meng, Q. S.; Yin, Q.; Tang, S.; Zhang, P. C.; Chen, Y.; Zhang, Z. W.; Yu, H. J.; Li, Y. P. Long circulation red-blood-cell-mimetic nanoparticles with peptide-enhanced tumor penetration for simultaneously inhibiting growth and lung metastasis of breast cancer. *Adv. Funct. Mater.* **2016**, *26*, 1243–1252.

[12] Parodi, A.; Quattrocchi, N.; van de Ven, A. L.; Chiappini, C.; Evangelopoulos, M.; Martinez, J. O.; Brown, B. S.; Khaled, S. Z.; Yazdi, I. K.; Enzo, M. V. et al. Biomimetic functionalization with leukocyte membranes imparts cell like functions to synthetic particles. *Nat. Nanotechnol.* **2013**, *8*, 61–68.

[13] Hu, C. M. J.; Fang, R. H.; Wang, K. C.; Luk, B. T.; Thamphiwatana, S.; Dehaini, D.; Nguyen, P.; Angsantikul, P.; Wen, C. H.; Kroll, A. V. et al. Nanoparticle biointerfacing by platelet membrane cloaking. *Nature* **2015**, *526*, 118–121.

[14] Hu, Q. Y.; Sun, W. J.; Qian, C. G.; Wang, C.; Bomba, H. N.; Gu, Z. Anticancer platelet-mimicking nanovehicles. *Adv. Mater.* **2015**, *27*, 7043–7050.

[15] Hu, Q. Y.; Bomba, H. N.; Gu, Z. Engineering platelet-mimicking drug delivery vehicles. *Front. Chem. Sci. Eng.* **2017**, *11*, 624–632.

[16] Sun, H. P.; Su, J. H.; Meng, Q. S.; Yin, Q.; Chen, L. L.; Gu, W. W.; Zhang, Z. W.; Yu, H. J.; Zhang, P. C.; Wang, S. L. et al. Cancer cell membrane-coated gold nanocages with hyperthermia-triggered drug release and homotypic target inhibit growth and metastasis of breast cancer. *Adv. Funct. Mater.* **2017**, *27*, 1604300.

[17] Hu, C. M. J.; Zhang, L.; Aryal, S.; Cheung, C.; Fang, R. H.; Zhang, L. F. Erythrocyte membrane-camouflaged polymeric nanoparticles as a biomimetic delivery platform. *Proc. Natl. Acad. Sci. USA* **2011**, *108*, 10980–10985.

[18] George, J. N. Platelets. *Lancet* **2000**, *355*, 1531–1539.

[19] Ho-Tin-Noé, B.; Demers, M.; Wagner, D. D. How platelets safeguard vascular integrity. *J. Thromb. Haemost.* **2011**, *9*, 56–65.

[20] Boilard, E.; Blanco, P.; Nigrovic, P. A. Platelets: Active players in the pathogenesis of arthritis and SLE. *Nat. Rev. Rheumatol.* **2012**, *8*, 534–542.

[21] Boilard, E.; Nigrovic, P. A.; Larabee, K.; Watts, G. F. M.; Coblyn, J. S.; Weinblatt, M. E.; Massarotti, E. M.; Remold-O'Donnell, E.; Farndale, R. W.; Ware, J. et al. Platelets amplify inflammation in arthritis via collagen-dependent microparticle production. *Science* **2010**, *327*, 580–583.

[22] Haynes, B. F.; Hale, L. P.; Patton, K. L.; Martin, M. E.; McCallum, R. M. Measurement of an adhesion molecule as an indicator of inflammatory disease activity: Up-regulation of the receptor for hyaluronate (CD44) in rheumatoid arthritis. *Arthritis Rheum.* **1991**, *34*, 1434–1443.

[23] Nedvetzki, S.; Walmsley, M.; Alpert, E.; Williams, R. O.;

Feldmann, M.; Naor, D. CD44 involvement in experimental collagen-induced arthritis (CIA). *J. Autoimmun.* **1999**, *13*, 39–47.

[24] Johnson, B. A.; Haines, G. K.; Harlow, L. A.; Koch, A. E. Adhesion molecule expression in human synovial tissue. *Arthritis Rheum.* **1993**, *36*, 137–146.

[25] Stone, J. P.; Wagner, D. D. P-selectin mediates adhesion of platelets to neuroblastoma and small cell lung cancer. *J. Clin. Invest.* **1993**, *92*, 804–813.

[26] Schett, G.; Gravallese, E. Bone erosion in rheumatoid arthritis: Mechanisms, diagnosis and treatment. *Nat. Rev. Rheumatol.* **2012**, *8*, 656–664.

[27] Brand, D. D.; Latham, K. A.; Rosloniec, E. F. Collagen induced arthritis. *Nat. Protoc.* **2007**, *2*, 1269–1275.

[28] Quan, L. D.; Zhang, Y. J.; Crielaard, B. J.; Dusad, A.; Lele, S. M.; Rijcken, C. J. F.; Metselaar, J. M.; Kostková, H.; Etrych, T.; Ulbrich, K. et al. Nanomedicines for inflammatory arthritis: Head-to-head comparison of glucocorticoid-containing polymers, micelles, and liposomes. *ACS Nano* **2014**, *8*, 458–466.

[29] Kim, M. J.; Park, J. S.; Lee, S. J.; Jang, J.; Park, J. S.; Back, S. H.; Bahn, G.; Park, J. H.; Kang, Y. M.; Kim, S. H. et al. Notch1 targeting siRNA delivery nanoparticles for rheumatoid arthritis therapy. *J. Control. Release* **2015**, *216*, 140–148.

[30] Allen, T. M.; Murray, L.; MacKeigan, S.; Shah, M. Chronic liposome administration in mice: Effects on reticuloendothelial function and tissue distribution. *J. Pharmacol. Exp. Ther.* **1984**, *229*, 267–275.

[31] Grozovsky, R.; Hoffmeister, K. M.; Falet, H. Novel clearance mechanisms of platelets. *Curr. Opin. Hematol.* **2010**, *17*, 585–589.

[32] Dehaini, D.; Wei, X. L.; Fang, R. H.; Masson, S.; Angsantikul, P.; Luk, B. T.; Zhang, Y.; Ying, M.; Jiang, Y.; Kroll, A. V. et al. Erythrocyte-platelet hybrid membrane coating for enhanced nanoparticle functionalization. *Adv. Mater.* **2017**, *29*, 1606209.

[33] Poduval, P.; Sillat, T.; Beklen, A.; Kouri, V. P.; Virtanen, I.; Konttinen, Y. T. Type IV collagen α-chain composition in synovial lining from trauma patients and patients with rheumatoid arthritis. *Arthritis Rheum.* **2007**, *56*, 3959–3967.

[34] Rosloniec, E. F.; Cremer, M.; Kang, A. H.; Myers, L. K.; Brand, D. D. Collagen-induced arthritis. *Curr. Protocols Immunol.* **2010**, *89*, 15.5.1–15.5.25.

[35] Schwartz, B. D.; Mengle-Gaw, L. J. Tacrolimus for the treatment of rheumatoid arthritis: Are broad-based immunosuppressants still valid? *Future Rheumatol.* **2006**, *1*, 661–672.

[36] Aryal, S.; Hu, C. M. J.; Fang, R. H.; Dehaini, D.; Carpenter, C.; Zhang, D. E.; Zhang, L. F. Erythrocyte membrane-cloaked polymeric nanoparticles for controlled drug loading and release. *Nanomedicine* **2013**, *8*, 1271–1280.

[37] Sintnicolaas, K.; van Marwijk Kooij, M.; van Prooijen, H. C.; van Dijk, B. A.; van Putten, W. L.; Claas, F. H.; Novotny, V. M.; Brand, A. Leukocyte depletion of random single-donor platelet transfusions does not prevent secondary human leukocyte antigen-alloimmunization and refractoriness: A randomized prospective study. *Blood* **1995**, *85*, 824–828.

[38] Hu, Q. Y.; Qian, C. G.; Sun, W. J.; Wang, J. Q.; Chen, Z. W.; Bomba, H. N.; Xin, H. L.; Shen, Q. D.; Gu, Z. Engineered nanoplatelets for enhanced treatment of multiple myeloma and thrombus. *Adv. Mater.* **2016**, *28*, 9573–9580.

[39] Hu, Q. Y.; Sun, W. J.; Qian, C. G.; Bomba, H. N.; Xin, H. L.; Gu, Z. Relay drug delivery for amplifying targeting signal and enhancing anticancer efficacy. *Adv. Mater.* **2017**, *29*, 1605803.

[40] Wang, C.; Sun, W. J.; Ye, Y. Q.; Hu, Q. Y.; Bomba, H. N.; Gu, Z. *In situ* activation of platelets with checkpoint inhibitors for post-surgical cancer immunotherapy. *Nat. Biomed. Eng.* **2017**, *1*, 0011.